Ab Initio Modeling of the Electronic Circular Dichroism Induced in Porphyrin Chromophores

Jiří Šebek[‡,†] and Petr Bouř*[,†]

Institute of Organic Chemistry and Biochemistry, Academy of Sciences, Flemingovo náměstí 2, 166 10 Prague 6, Czech Republic, and Department of Analytical Chemistry, Institute of Chemical Technology, Technická 5, 166 28 Prague 6, Czech Republic

Received: December 1, 2007; In Final Form: January 18, 2008

The optical activity in porphyrins can easily be induced by a chiral environment, but it is difficult to determine the underlying mechanisms purely on an experimental basis. Therefore, in this study, magnitudes of the perturbational, dipolar, and direct covalent contributions to the electronic circular dichroism (CD) are evaluated with the aid of quantum chemical computations. Electronic properties of model porphyrin chromophores are analyzed. Time-dependent density functional theory (TD DFT), particularly with the hybrid B3LYP functional, appeared suitable for estimation of the electronic excitation energies and spectral intensities. The transition dipole coupling (TDC) between chirally stacked porphyrins was determined as the most important mechanism contributing to their optical activity. This is in agreement with previous experimental observations, where chiral matrices often induce the stacking and large CD signals. About a 10 times smaller signal could be achieved by a chiral orientation of the phenyl or similar residues covalently attached to the porphyrin core. Also, this prediction is in agreement with known experiments. Perturbation models realized by a chirally arranged porphyrin and a point charge, or by a porphyrin and the methane molecule, provided the smallest CD signals. The electrically neutral methane induced similar CD magnitudes as those of the charge, but spectral shapes were different. For a complex of porphyrin and the alanine cation, a significant influence of the solvent on the resultant CD spectral shape was observed, while for the charge and methane perturbations, a negligible solvent effect was found. Detailed dependence of the induced optical activity on variations of geometrical parameters is discussed. The simulations of the induced porphyrin activity can thus bring important information about the structure and intermolecular interactions in chiral complexes.

Introduction

Porphyrins and porphyrin-like compounds always attract attention as natural pigments important for metabolic cycles. They can be used in electronics, optical devices, and many other applications.[1,2] Conjugates with polypeptides are utilized in the photodynamic cancer therapy as photosensitizing agents.[3] Due to the ability of the porphyrin core to absorb visible light, optical spectroscopies belong to the primary methods used for elucidation of porphyrin structure as well as interactions with other compounds. For example, chiral spectroscopic methods were used for monitoring of porphyrin binding to peptides,[3,4] nucleic acids,[5] or chiral dendrimer structures.[6]

The differential circular dichroic spectroscopy is an especially convenient tool for the porphyrin complexation studies. It brings enhanced structural information if compared to the unpolarized absorption, sensitive to molecular chirality.[1,7,8] Moreover, although porphyrin cores often possess high symmetries and are not optically active, the activity can be induced by a presence of peptide[3,9] or nucleic acid[10,11] matrices, or it can be due to covalently bound substituents.[4,12] Then, the induced dichroism allows one to monitor both porphyrins and the chiral counterparts.[13,14] Ideally, signals of porphyrins and chiral biopolymers do not overlap; one spectral record provides independent information about both constituents. More frequently, the resolution of the porphyrin and matrix components in the spectra is achieved by a combination of vibrational and electronic techniques.[3,15]

Possible origins of the optical activity in achiral systems were discussed a long time ago.[4,16−18] However, the roles of various mechanisms in real systems are not clear as detailed geometries of porphyrin−polymer aggregates are often not known. The large sizes of investigated systems prevent precise quantum chemical modeling.[4] For some chromophores, semiempirical rules for determination of the CD signs were proposed.[19,20] These were found to be unreliable in general. It was only after the formulation of the time-dependent density functional theory (TD DFT)[21] and its implementation into common quantum chemical programs[22,23] when CD spectra of medium-sized systems could be calculated with a reasonable precision.[22,24−26] On the other hand, black box quantum computations often do not provide the intuitive insight of the simpler empirical models.

Therefore, in this study, we briefly review previously proposed mechanisms of the induction of optical activity in achiral groups. Then, TD DFT computations are used to estimate relative magnitudes and shapes of the circular dichroic signals induced in variously perturbed or chirally arranged porphyrins. The relation between the spectra and the structure is important from the experimental point of view since the CD often provides the only information about the system geometry. It appears that an excitonic mechanism associated with stacking and interaction

* To whom correspondence should be addressed. E-mail: bour@uochb.cas.cz.
† Academy of Sciences.
‡ Institute of Chemical Technology.

10.1021/jp711364j CCC: $40.75
Published on Web 03/06/2008

of more porphyrin chromophores produces the largest CD signal observed in common experiments.

Porphyrin Optical Activity

Several standard models were proposed to explain the porphyrin optical activity.[16,17] Typically, the porphyrin chromophore alone possesses at least three symmetry planes and, as such, is not optically active. In many cases, the perturbational theory is suitable to describe the role of a chiral environment; unperturbed porphyrin wave functions $\varphi_i = |i\rangle$ and Hamiltonian H oblige the Schrödinger equation, $H\varphi_i = e_i\varphi_i$, where e_i are the state energies, whereas the chirality is induced by an external perturbation V. This causes mixing of the states φ_i and lowering of the porphyrin symmetry. We restrict ourselves to systems of D_{2h} symmetry and others that do not contain degenerate states. Then, the mixing coefficients t_{ij} at various orders can be obtained from the standard perturbation expansions. Particularly, new perturbed states can be then written as

$$|i'\rangle = |i\rangle + \sum_{j\neq i}\frac{V_{ji}}{e_i - e_j}|j\rangle + \sum_{j\neq i}\sum_{j'\neq i}\left(\frac{V_{jj'}V_{j'i}}{e_i - e_{j'}} - \frac{V_{ji}V_{jj}}{e_i - e_j}\right)\frac{1}{e_i - e_j}|j\rangle + ... = |i\rangle + \sum_{j\neq i}t_{ij}^{(1)}|j\rangle + \sum_{j\neq i}t_{ij}^{(2)}|j\rangle + ... = |i\rangle + \sum_{j\neq i}t_{ij}|j\rangle \quad (1)$$

where $V_{ji} = \langle j|V|i\rangle$. Induced rotational strength for a transition $i' \rightarrow j'$ up to the second power of the mixing coefficients t_{ij} becomes

$$R' = \mathrm{Im}\langle i'|\boldsymbol{\mu}|j'\rangle\cdot\langle j'|\mathbf{m}|i'\rangle = \mathrm{Im}[\boldsymbol{\mu}_{ij}\cdot(\sum_{k\neq i}t_{ik}\mathbf{m}_{jk} + \sum_{k\neq j}t_{jk}^{*}\mathbf{m}_{ki} + \sum_{k\neq j}\sum_{k'\neq i}t_{jk}^{*}t_{ik'}\mathbf{m}_{kk'}) + (\sum_{k\neq j}t_{jk}\boldsymbol{\mu}_{ik} + \sum_{k\neq i}t_{ik}^{*}\boldsymbol{\mu}_{kj} + \sum_{k\neq i}\sum_{k'\neq j}t_{ik}^{*}t_{jk'}\mathbf{m}_{kk'})\cdot\mathbf{m}_{ji} + \sum_{k\neq j}t_{jk}\boldsymbol{\mu}_{ik}\cdot\sum_{k\neq i}t_{ik}\mathbf{m}_{jk} + \sum_{k\neq j}t_{jk}\boldsymbol{\mu}_{ik}\cdot\sum_{k\neq j}t_{jk}^{*}\mathbf{m}_{ki} + \sum_{k\neq i}t_{ik}^{*}\boldsymbol{\mu}_{kj}\cdot\sum_{k\neq i}t_{ik}\mathbf{m}_{jk} + \sum_{k\neq i}t_{ik}^{*}\boldsymbol{\mu}_{kj}\cdot\sum_{k\neq j}t_{jk}^{*}\mathbf{m}_{ki} + o(t^3)] \quad (2)$$

where $\boldsymbol{\mu}$ and $\mathbf{m}$ are the electric and magnetic dipole moments and the transition integrals are abbreviated, for example, $\mathbf{m}_{ij} = \langle i|\mathbf{m}|j\rangle$. Particularly for a part proportional to the first power of the potential, we get

$$R' \cong \mathrm{Im}\left(\boldsymbol{\mu}_{ij}\cdot\left[\sum_{k\neq i}\frac{V_{ki}\mathbf{m}_{jk}}{e_i - e_k} + \sum_{k\neq j}\frac{V_{jk}\mathbf{m}_{ki}}{e_j - e_k}\right] + \left[\sum_{k\neq j}\frac{V_{kj}\boldsymbol{\mu}_{ik}}{e_j - e_k} + \sum_{k\neq i}\frac{V_{ik}\boldsymbol{\mu}_{kj}}{e_i - e_k}\right]\cdot\mathbf{m}_{ji}\right) \quad (3)$$

A point charge q placed at a position $\mathbf{r}$ represents one of the simplest perturbations. The potential operator is then

$$V = -e\sum_{l=1...N}\phi(r_l) \quad (4)$$

where $\phi(r_l) = (1/4\pi\epsilon_0)(q/(|\mathbf{r} - \mathbf{r}_l|))$, $\mathbf{r}_l$ is the position of an electron, e is its charge, and ϵ_0 is the vacuum permittivity. The validity of the perturbation modeling can be judged from the properties of ab initio computations. For example, the linear formula (eq 3) predicts opposite strengths for opposite charges, $R'(q) = -R'(-q)$. Moreover, the potential within the chromophore can be expanded into multipoles related to the origin **o**

$$V_{ji} = \mu_{ji}\cdot\nabla\phi(\mathbf{o}) + \Theta_{ji}\cdot\cdot\nabla\nabla\phi(\mathbf{o}) + ... \quad (5)$$

Then, from eq 3, we obtain distance dependences of the strength on the dipolar ($R \sim 1/r^2$) and quadrupolar ($R \sim 1/r^3$) contributions, with r being the distance between the charge and the chromophore.

Instead of the charge, a sphere characterized by polarizability α would cause a similar perturbation. This case is more complicated than the charge; if only the electron potential is considered, a fourth-power decay ($R \sim 1/r^4$) is obtained from eq 3. Higher powers of $1/r$ are likely for a higher-order perturbational mechanism indicated in eq 2. However, it is important to note that different combinations of the multipolar terms and perturbational orders can lead to the same distance dependence of the strength. Only the lowest possible exponent of $(1/r)$ can reliably be predicted by the perturbational calculus.

A substituent covalently bound to the porphyrin chromophore can also perturb and mix the porphyrin electronic states. For example, we obtain chiral dyes by rotation of the methyl or phenyl residues in the tetramethylporphyrin (TMP) and tetraphenylporphyrin (TPP; see Figure 1). In this case, however, the changes in the electronic structures might be quite complex and cannot be approximated by simple mathematical expressions. On the other hand, it is known that the porphyrin chromophore conserves its basic characteristic in a broad variety of derived compounds,[27] and the perturbation concept on a qualitative level still enhances understanding of the light-scattering properties.

Finally, dimerization and stacking of many achiral molecules in a presence of chiral matrices can also lead to the optical

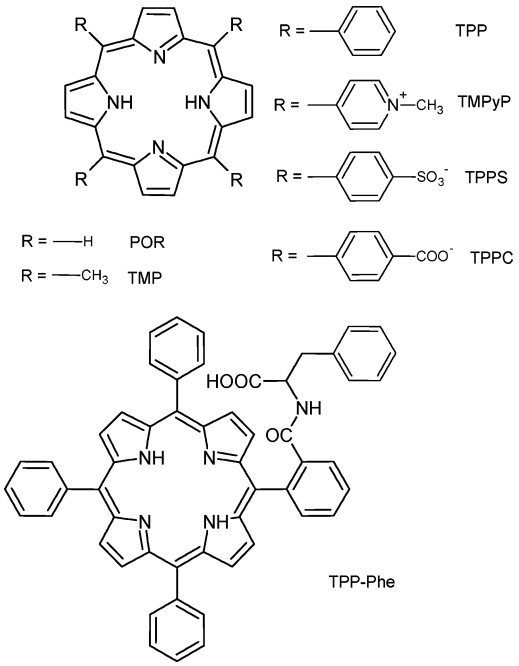

Figure 1. Porphyrin derivatives studied in this work: porphine (porphyrin, POR), tetramethylporphine (TMP), tetraphenylporphine (TPP), cationic *meso*-tetrakis(*N*-methylpyridinium-4-yl)porphine (TMPyP), anionic 5,10,15,20-tetraphenyl-21H,23H-porphine-*p*,*p*′,*p*″,*p*‴-tetrasulfonate (TPPS) and 5,10,15,20-tetraphenyl-21H,23H-porphine-*p*,*p*′,*p*″,*p*‴-tetracarboxylate (TPPC), and the TPP with a covalently bound phenylalanine residue (TPP−Phe).

TABLE 1: Calculated Wavelengths and Dipole Strengths of the Lowest-Energy Porphyrin Transitions

transition symmetry	B-LYP 6-31G*	B-P 6-31G*	B3LYP 6-31G*	B3LYP 6-31G*[b]	B3LYP 6-311++G**	B3LYP05 6-311++G**	exp[a]
			(a) Wavelengths (nm)				
1 B_{2u}	582	577	551	545	555	572	617
2 B_{1u}	547	543	514	511	520	539	521
3 B_{2u}	421	419	377	370	380	408	400
4 B_{3g}	429	427	368	362	370	410	
5 B_{1u}	416	414	357	352	364	399	400
6 A_g	421	419	349	341	351	400	
7 B_{1u}	362	361	333	329	337	363	
8 B_{2u}	356	355	325	324	331	354	
			(b) Dipole Strengths (debye^2)				
1 B_{2u}	16	17	1	4	0	8	
2 B_{1u}	8	9	0	1	0	4	
3 B_{2u}	915	927	3180	3238	3788	1669	
4 B_{3g}	0	0	0	0	0	0	
5 B_{1u}	213	213	4529	5077	5544	768	
6 A_g	0	0	0	0	0	0	
7 B_{1u}	6463	6384	3791	3325	3212	7123	
8 B_{2u}	5496	5444	5438	5376	5153	5992	

[a] Refs 27 and 37. [b] With the solvent (water) CPCM correction. All computation were done with the BPW91/6-31G* equilibrium geometry.

activity of the porphyrins.[3,4,6] In this case, the transition dipole coupling (TDC) is the most likely mechanism.[18,28] Porphyrin dipole transitions interact, and the electronic levels split. Moreover, the dipoles of mutually fixed positions provide the magnetic moment. Consequently, the nonzero rotational strength and the CD spectrum arise. In the more advanced matrix method,[29,30] higher-order interactions might be considered. In this study, we can concentrate on the presumably dominant dipole−dipole contribution, where the splitting of the energy levels of oscillators i and j with transition dipoles $\boldsymbol{\mu}_i$ and $\boldsymbol{\mu}_j$ is given by

$$W_{ij} = \frac{1}{4\pi\epsilon} \frac{\boldsymbol{\mu}_i \cdot \boldsymbol{\mu}_j r_{ij}^2 - 3\boldsymbol{\mu}_i \cdot \mathbf{r}_{ij} \boldsymbol{\mu}_j \cdot \mathbf{r}_{ij}}{r_{ij}^5} \tag{6}$$

where ϵ is the electric permittivity and $\mathbf{r}_{ij}$ the distance vector. Resultant excited states

$$\Psi_J = \sum_i c_{Ji} \varphi_i$$

are obtained by diagonalization of the corresponding Hamiltonian; the function φ_i represents a monoexcited oscillator i of frequency ω_i. The dipole and rotational strength to the transition J are then given by[18,28,31]

$$D_J = |\sum_i c_{Ji} \boldsymbol{\mu}_i|^2 \tag{7}$$

and

$$R_J = (\sum_i c_{Ji}^* \boldsymbol{\mu}_i) \cdot \left(\frac{1}{2} \sum_j \omega_j c_{Jj} \mathbf{r}_j \times \mathbf{m}_j \right) \tag{8}$$

Computations

Equilibrium geometries of various porphyrin derivatives (Figure 1) were obtained by energy minimization at the BPW91[32]/6-31G* level. The electronic excited-state properties were obtained within the time-dependent density functional approach, typically at the B3LYP[33]/6-31G* level. As found before,[34] the B3LYP functional provides almost the same geometries but notably better electronic spectra than those of the B-P or BPW91 methods. Both Turbomole[35] and Gaussian[36] program packages were used for the computation as they provided practically indistinguishable results. The transition energies and dipole moments of monomeric porphyrin were also used in the transition dipole coupling scheme for simulation of the porphyrin complexes. Absorption and CD spectra were generated from the calculated dipole and rotational strengths using Lorentzian bands with a full width at half-height of 15 nm.

Results and Discussion

Electronic Transitions in the Porphyrin Chromophore. Sensitivity of the results on the basis set size and the DFT approximation was estimated for the unsubstituted porphyrin (POR, Figure 1). Energies and dipole strengths of eight lowest-energy transitions computed at different levels are listed in Table 1. Reasonable transition wavelengths (part a of the Table) are obtained by all of the calculations. The highest band wavelength (absorption threshold), experimentally at ~ 617 nm, is slightly underestimated by all of the methods. The GGA functionals (B-LYP, B-P) tend to provide higher transition wavelengths than the hybrid B3LYP functional explicitly containing the HF exchange. The GGA wavelengths of the most intense Soret bands are ~20 nm higher and the B3LYP values are ~35 nm lower that the experimental band reported at ~400 nm.[27,37] The B3LYP05 functional previously recommended for computations of NMR properties[38,39] contains less HF exchange. It was also supposed to provide better excitation energies than the original B3LYP parametrization. Indeed, it provides an overall improvement in the entire spectral region.

On the other hand, the energies seem to be fairly independent of the basis set size; at least the 6-31G* → 6-311++G** basis extension at the B3LYP level produces rather negligible wavelength changes in comparison to the absolute error. We realize that used basis sets are not complete and certainly cannot account for all possible transitions, especially those including the Rydberg states. Fortunately, these do not seem to be important for the valence transitions in the longer-wavelength region important in most practical applications.

Similarly as the energies, the dipole strengths (part b of Table 1) do not significantly depend on the basis set size. However, the functional dependence is more dramatic than that for the energies. For the third Soret region transition, for example, about 25% of the B3LYP intensity is obtained by the GGA methods,

TABLE 2: Calculated (B3LYP/6-31G*) Excitation Wavelengths and Dipolar Strengths for Several Porphyrin Derivatives

transition	POR[a]	TMP[a]	TPP[a]	TPPC	TPPS	TMPyP
			Wavelength (nm)			
1 B_{2u}	551	604	573	590	595	601
2 B_{1u}	514	545	534	554	558	571
3 B_{2u}	376	393	394	403	407	426
4 B_{3g}	368	386	380	370	374	411
5 B_{1u}	357	372	375	327	344	394
6 A_g	348	346	358	353	355	403
7 B_{1u}	333	333	347	327	344	394
8 B_{2u}	324	340	341	325	342	398
9 B_{3g}	310	342	320	335		
			Dipole Strengths (10^{-2} D^2)			
1 B_{2u}	1	388	104	706	785	97
2 B_{1u}	0	64	145	1056	1382	784
3 B_{2u}	3180	3494	5461	9471	1395	170
4 B_{3g}	0	0	0	0	0	0
5 B_{1u}	4529	7741	9140	2475	1344	15
6 A_g	0	0	0	2	0	0
7 B_{1u}	3791	1254	2752	2475	1344	15
8 B_{2u}	5438	4926	6813	3145	4005	55
9 B_{3g}	0	0	0	0		

[a] D_{2h} symmetry was enforced.

whereas the GGA dipole strength of the first transition is 16−17 times bigger. Also, the seemingly small difference between the B3LYP and B3LYP05 functionals leads to significant changes in the dipolar strengths of most transitions. The CPCM solvent correction (fifth column in Table 1) caused only minor changes of the spectral parameters, unlike that for strongly polar systems observed in previous studies.[34,40,41] This reflects the low polarity of the hydrophobic porphyrin chromophore. Experimental strengths resolved for individual transitions are not available to us; nevertheless, the magnitudes and relative ratios of the computed dipole strengths correspond well to the condensed-phase experiments.[27,37] Overall, we can conclude that for the purpose of this study, all of the methods reproduce basic electronic features of the porphyrin chromophore.

For the computations presented below, the standard B3LYP functional is preferred. At this stage, we do not see the better performance of the B3LYP05 functional for energies as a sufficient proof of its performance. Better agreement of the frequencies was achieved by an empirical fit, and the performance for the intensities may not be so reliable. In any case, the selection of a particular functional does not seem to be important for the behavior of the porphyrin chromophore pursued in this study. Longest-wavelength (lowest-energy) transitions down to about 320 nm are calculated; therefore, the zero spectra below this wavelength might not be real.

Porphyrin Derivatives. The dependence of the absorption spectra on the substitution of the porphyrin chromophore was investigated for the unsubstituted porphyrin (POR), tetramethylporphyrin (TMP), tetraphenylporphyrin (TPP), tetraphenylporphyrincarboxylate (TPPC), tetraphenylporphyrinsulfate (TPPS), and tetramethylpyridiniumporphyrin (TMPyP) compounds (Figure 1). The transitions in the unsubstituted chromophore (POR) were semiautomatically assigned to those in the porphyrin derivatives on the basis of the overlap of corresponding molecular orbitals.[34] As expected, fundamental porphyrin electronic properties were not changed dramatically by the substitutions. Particularly for most of the lowest-energy POR transitions, counterparts could also be found in the other porphyrin derivatives (Table 2). For example, the calculated transition energies of the methylated porphyrin (TMP) closely follow those of the unsubstituted compound. The lowest-energy (highest-wavelength) band is the most sensitive to the methyl substitution, changing its wavelength by about 10% (551 → 604 nm). Moreover, making the substituents bigger in the tetraphenylporphyrin (fourth column) changes the energies even less if compared with the methyl analogue. The energy of the Soret transitions (numbers 3 and 5) differ by less than about 3 nm. Even the charged residues (COO^-, SO_3^-, and Py^+) do not cause significant energy shifts in TPPC, TPPS, or TMPyP, although here, the character of the transition changes, and some POR transitions could not be assigned unambiguously. At least for the lowest-energy transitions, however, the local change consisting of the replacement of the POR hydrogen by the first carbon of the substituents causes the biggest perturbation of the energies.

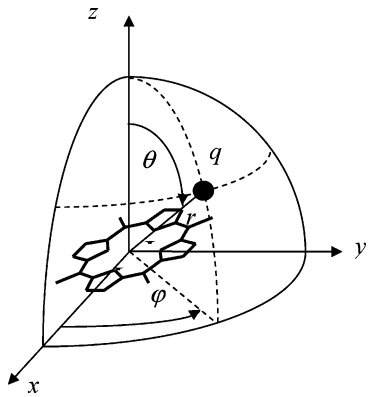

Figure 2. Position of the point charge q with respect to the porphyrin aligned in the xy plane is defined in polar coordinates by the (θ, φ) angles and the r distance.

The dipole strengths of the derivatives listed in the lower part of Table 2 vary more than the energies. For example, the strength of the lowest-energy transition is significantly smaller in the unsubstituted compound POR, while its magnitude is increased by two orders in TMP and TPP. Interestingly, the negatively charged residues in TPPC and TPPS tend to increase or conserve the dipole strengths, while for the positively charged TMPyP compound, the strengths are, on average, smaller if related to the nonpolar compounds (POR, TPP, and TMP). This can be explained in terms of electron conjugation effects. The positive residues in TMPyP drag electrons out from the porphyrin chromophore, restrict their motion, and consequently, restrict the dipole strengths in the lowest-energy spectral region. The methylated porphyrin still appears as a best minimal model for the most common experimental systems, where the hydrogens on the methine −C═ bridge are always substituted in order to gain solubility or complexation affinity. However, the variations in Table 2 confirm that porphyrin absorption properties can still be tuned by the substituents, especially those containing the polar groups.

The Perturbation Mechanism. In order to investigate the optical activity caused by a simple perturbation, a point charge was positioned near the TMP chromophore. The absorption and CD spectra of this system were calculated ab initio at the B3LYP/6-31G** level. The charge positions were varied within the octant described by the polar coordinates in Figure 2. In Figure 3, we can follow the dependence of the rotational strengths of the most-intense Q band (∼610 nm) and Soret (∼380 nm) transitions on the geometry parameters and charge size. From the θ dependence (upper left graph in Figure 3, for constant distance and the φ angle), we can see that the perturbation is amplified namely when the charge approaches

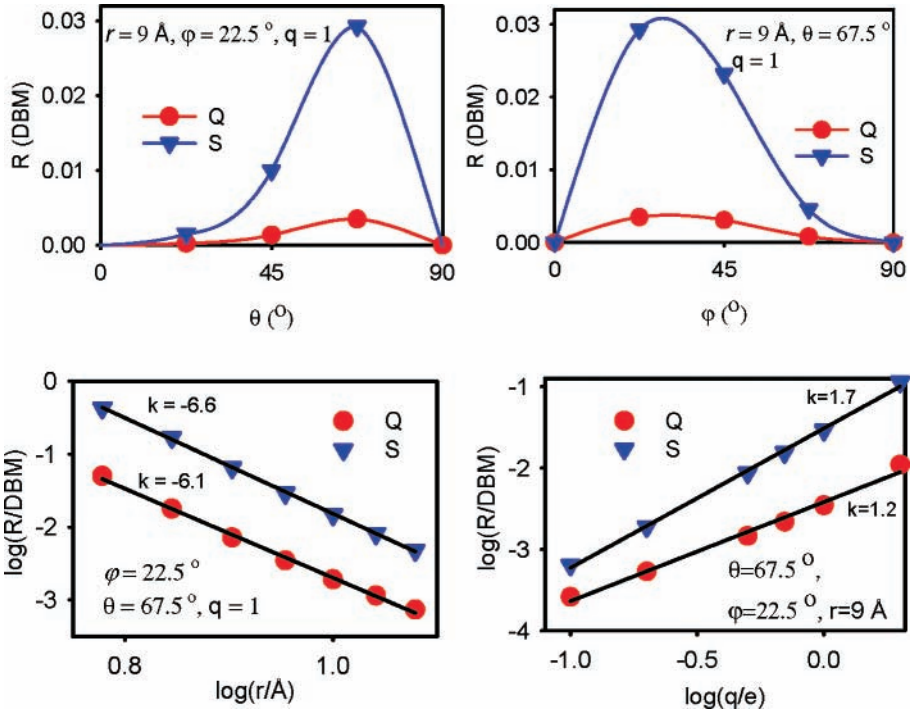

Figure 3. Dependence of the rotational strength (R) induced in TMP on the position and size of the unit charge defined in Figure 2 (B3LYP/631-G**, Q band ~ 610 nm, S band ~ 380 nm). The slopes of the linear dependencies were obtained by a linear fit ($y = kx + c$).

the porphyrin plane, and the maximum of the optical activity is achieved for $\theta \sim 67.5°$. This may be expected because the π electrons in the porphyrin can certainly be polarized more easily along the plane than in a perpendicular direction. Perhaps more surprisingly, for constant θ, the φ dependence (upper right graph in the figure) is not symmetric either; in this case, however, the asymmetry induced by the middle hydrogen atoms causes the maximum strength to be at $\varphi \sim 30°$, much closer to the middle 45° value.

The distance and charge dependences at the lower part of Figure 3 are plotted on the logarithmic scale. The sharp decay of the strength with the distance ($\sim\mathbf{r}^{-6.1}$ for the Q band and $\sim\mathbf{r}^{-6.6}$ for the Soret band, as determined by the linear extrapolation coefficients k in the figure) allows us to exclude the linear formula (eq 3) as the dominant mechanism of the induction. Most probably, other terms in eq 2 proportional to the second power of the interaction potential provide the biggest contribution to the induced optical activity. This is also partially supported by the dependence of the strengths on the charge (lower right panel in Figure 3). It is not linear either, but the strength scales as $\sim q^{1.2}$ and $\sim q^{1.7}$ for the Q and Soret bands, respectively. Overall, we can conclude that rather a complex nonlinear perturbation of the porphyrin electronic structure takes place in the presence of the point charge.

The complexity is documented also in Figure 4, where three selected TMP orbitals (91 = HOMO-6 (B_{1u}), 96 (A_u), and 98 (B_{2g})) are plotted as calculated at the B3LYP/CPCM(H_2O)6-31G* level with and without the charge. The perturbed orbitals are also compared to a corresponding vacuum calculation; unperturbed vacuum and PCM orbital shapes do not change significantly. We can see two instructive effects. First, the solvent significantly shields the charge effect and, for the same geometry, leads to smaller orbital shape perturbations than those observed for vacuum. Second, the B_{1u} orbital with one nodal plane is effected more by the charge than B_{2g} (two nodal planes), while the A_u (three planes) shape is virtually unchanged, even in vacuum. This corresponds to the multipole expansion of the charge field (eq 5) and can also be followed by the magnitudes of the orbital energy shifts. For the case of TMP in vacuum, for example, all orbital energies are, on average, lowered by about 0.06 hartree by the presence of the charge. The energies of the B_{1u}, B_{2g}, and A_u orbitals selected in Figure 4 further differ by 0.0024, −0.0013, and −0.0002 hartree from this averaged value, respectively, and thus quantitatively reflect the importance of the dipolar, quadrupolar, and octopolar interactions.

Surprisingly, despite this complexity, the approximate proportionality of the chirality to the charge is partially conserved. In Figure 5, CD and absorption TMP spectra were simulated for positive and negative unit charges. The CD spectrum (top of the Figure) completely changes sign when the charge is inversed, although the plus and minus intensity patterns are symmetric only roughly. This suggests that odd terms in the perturbation expressions above, such as terms linear and cubic in the interaction potential, substantially contribute to the rotational strength. The sharp distance dependence actually suggests that the simple eq 3, although it provides a good conceptual basis, might not be completely adequate for the detailed description of the mechanism. For the absorption spectra (lower part of Figure 5), we can find examples when the changes caused by the charge might be caused predominantly by an even term (e.g., proportional to the square of the charge), such as the band at ~340 nm, where the intensity diminishes for both positive and negative charges if compared to the unperturbed TMP (green line). However, for the highest intensity ($\lambda \sim 380$ nm) and the Q bands (at ~550 and 610 nm), the odd terms seem to dominate as the highest, middle, and lowest intensity corresponds to the positive, zero, and negative charges, respectively.

Interestingly, the methane that can be thought of as a polarizable sphere produces quite a different, conservative CD shape that can be seen in the upper part of Figure 6. The strongest transitions (B_{1u} and B_{2u} bands in the Q and Soret region; see also Table 2) provide split, approximately conservative bands. This externally mediated coupling thus reminds one of the transition coupling scheme; here, however, two transitions (polarized in the x and y axes lying in the porphyrin plane) that

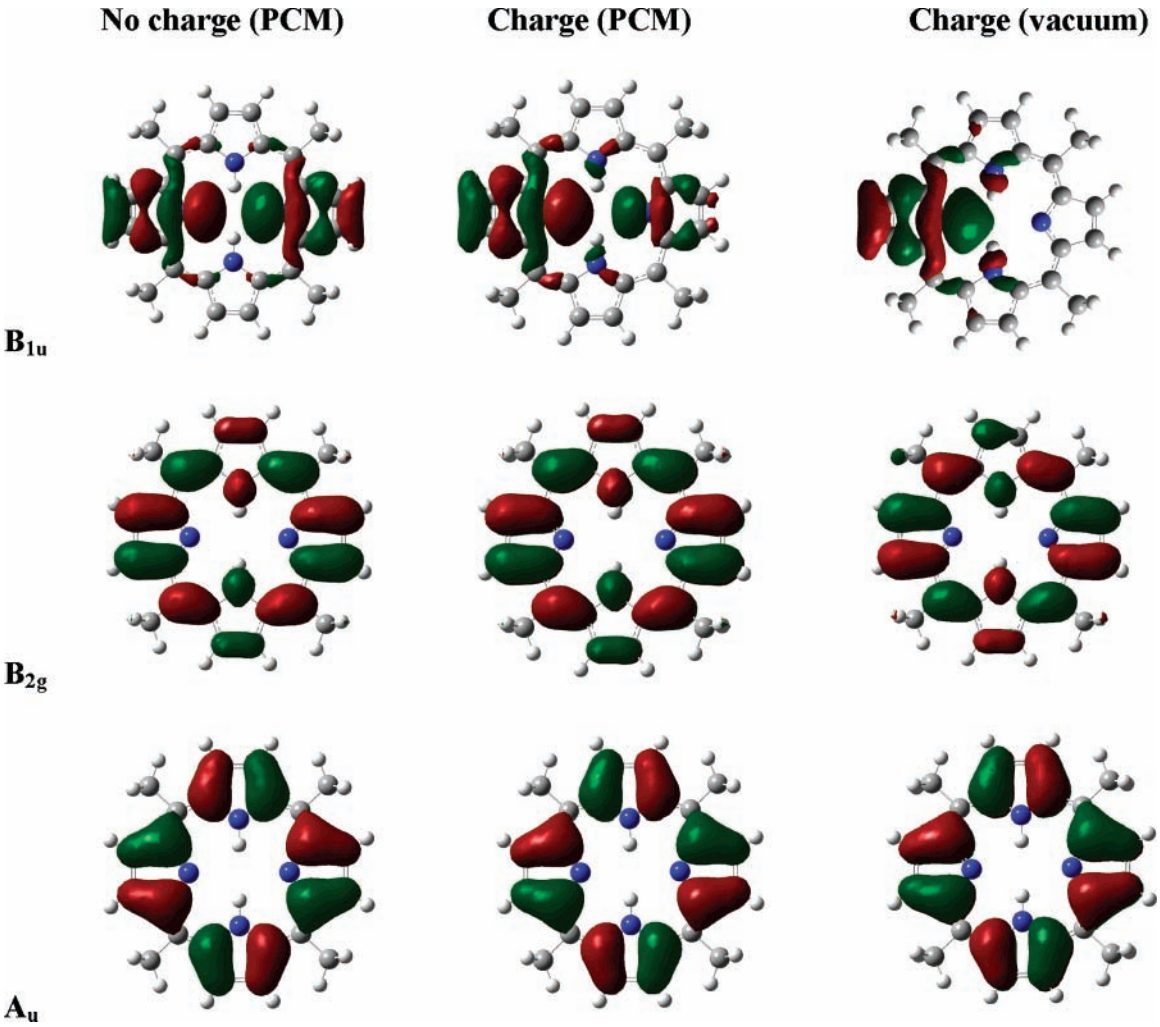

Figure 4. Example of TMP orbitals unperturbed (left) and perturbed in the solvent (middle) and vacuum (right) by the presence of a unit point charge ($r = 9$ Å, $\varphi = 22.5°$, $\theta = 67.5°$).

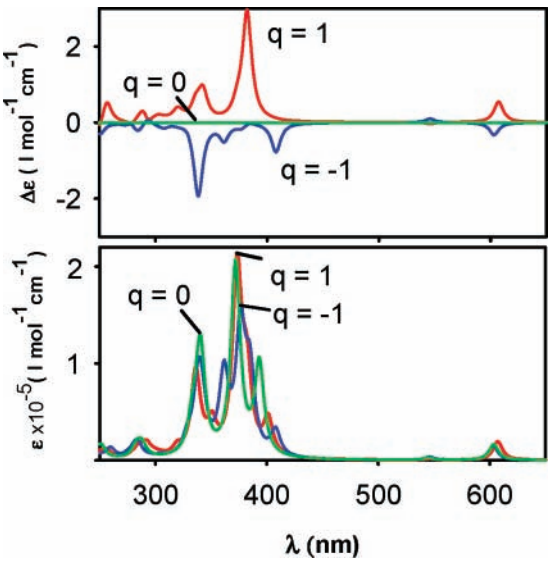

Figure 5. Calculated CD (top) and absorption (bottom) spectra induced in TMP (D_{2h}) by positive and negative unit charges ($r = 9$ Å, $\theta = 67.5°$, $\varphi = 22.5°$).

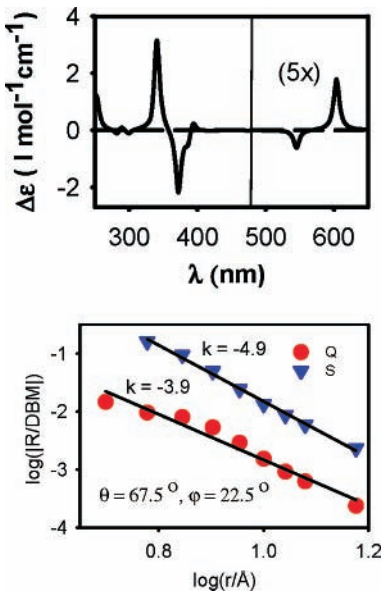

Figure 6. Calculated CD spectrum induced in TMP by the methane molecule (top, $\theta = 67.5°$, $\varphi = 22.5°$, B3LYP/ 6-31G**) and the dependence of the strengths of the most-intense Q and S bands on the distance (bottom).

belong to the same chromophore are coupled with the aid of another, not directly absorbing molecule. According to our knowledge, this phenomenon has never been studied before.

The dependence of the rotational strength for the selected Q and Soret transitions in TMP on the distance of the methane molecule can be seen in the lower part of Figure 6. Unlike for the charge (Figure 3), the logarithmic scale does not provide straight lines within the interval of investigated distances. The

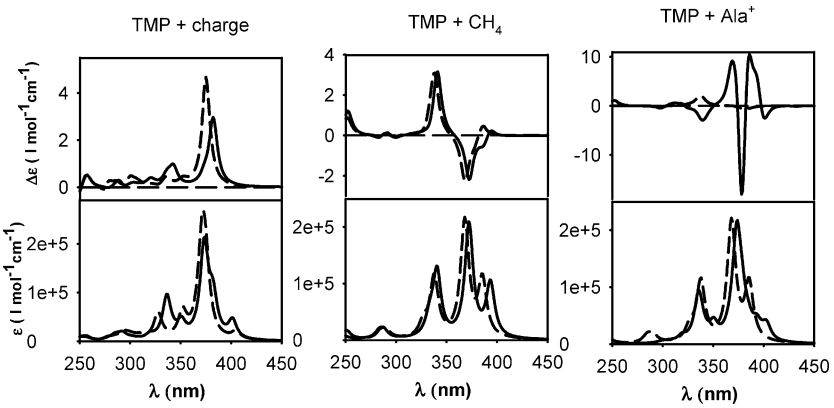

Figure 7. Calculated CD (top) and absorption (bottom) TMP spectra induced by the unit charge (left), methane (middle), and cationic alanine (right) molecules placed approximately at the same position (θ=67.5°, φ=22.5°, r = 9 Å, B3LYP/ 6-31G**) in vacuum (solid lines) and in water (simulated by the COSMO model, dashed lines).

distance dependence thus is more complicated than a simple power function (r^k). However, the approximate average exponents (−4.9 and −3.9) are smaller in absolute value than those for the charge, which is rather unusual as the polarization effects are usually considered to be much weaker and decay much faster with the distance than those connected with the charge field. We explain this effect by the exciton coupling of the energetically semidegenerate porphyrin states mediated by the methane. The magnitudes of the CD signals induced by the charge and methane, if placed at comparable distances, are nevertheless comparable.

For the simple perturbations realized by the charge and methane, relatively small changes in the CD and absorption spectra are caused by the solvent. This can be seen in Figure 7, where the vacuum spectra are compared to those obtained with the COSMO (H_2O) solvent correction. However, if the positively charged alanine molecule is used as the perturbation (right-hand panel in Figure 7), the induced vacuum CD signal almost diminishes. This volatility can be explained by a larger-scale electron redistribution within the polar alanine caused by the solvent, as well as by the shielding effect of the dielectric damping the electrostatic interaction between the porphyrin and the amino acid.

In order to estimate the possible relaxation of the TMP geometry under the presence of the charge and its effect on the induced spectra, in a control computation (not shown), the TMP molecule was anchored in space by three atoms and otherwise allowed to fully relax at the BPW91/6-31G** level. The relaxation caused a minor nonplanar deformation of the porphyrin core. However, within the region of 360−800 nm, computed changes in induced CD spectra were rather insignificant (e.g., ∼20% increase in the Soret band intensity). Thus, the static geometry model appears justified as a first approximation to the perturbational models. However, the deformation causes more extensive spectral variations in the higher-energy region (wavelengths < 350 nm).

Covalently Bound Substituents. In Table 2, we saw that groups covalently attached to the porphyrin ring can significantly influence transition energies and absorption intensities. In order to estimate their influence on the optical activity and magnitude of the CD signal, we simulated (B3LYP/6-31G**) CD spectra of the TPP derivative with the phenylalanine residue. The minimal-energy TPP−Phe structure (bottom panel in Figure 8) provides a relatively large CD signal ($\Delta\epsilon_{max} \sim 10^2$) if compared to the systems with the charges and the methane molecule placed at a reasonable distance. Note that the influence of the three unsubstituted phenyl groups in TPP−Phe was zeroed out by

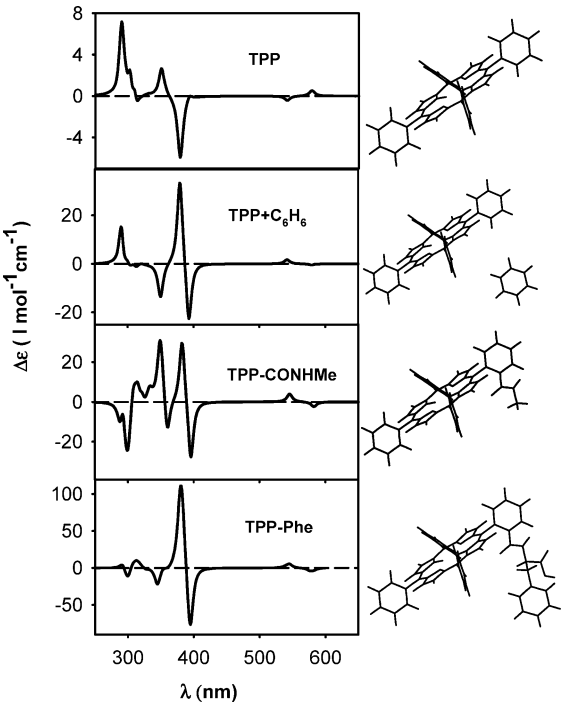

Figure 8. From top to bottom: CD spectra of a chiral TPP conformation, TPP complex with benzene, TPP−CONHMe, and TPP−Phe derivatives. The geometries of all systems are derived from TPP−Phe without optimization.

averaging the signal from all optically active conformers. Thus, the chirality comes exclusively from the chirally oriented phenylalanine residue. In the experiment, the signal can become smaller due to conformational flexibility. Nevertheless, we suppose that our model based on the equilibrium conformation reasonably approximates at least the magnitude of the induced CD. The peptide and benzene chromophores themselves absorb below 300 nm and should not interfere with the porphyrin signal within the plotted range.

The origin of the TPP−Phe optical activity appears to be relatively complex, which is partially demonstrated in the spectra of simplified models plotted in the other parts of Figure 8. The chiral position of the phenyl residue (TPP, when rotation of the other three was averaged out; the top panel in the Figure) provides a notable CD signal, which, in the Soret region, even copies the shape of TPP−Phe. However, the CD signal for the Q bands is opposite, and most importantly, the overall magnitude of the TPP CD ($\Delta\epsilon_{max} < 10^1$) is smaller by a factor of 10 than that for the original TPP−Phe compound. The CD signal can

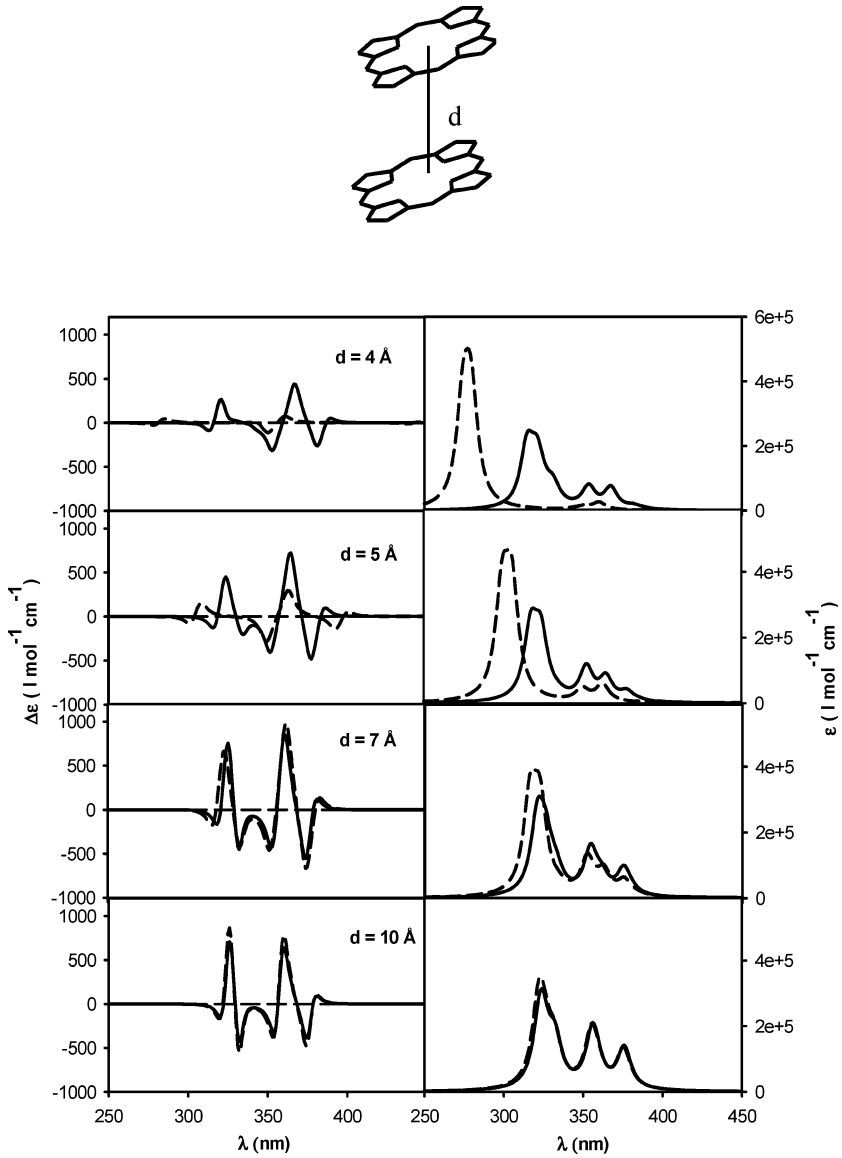

Figure 9. Parallel POR dimer (twisted by 45°), distance dependence of the CD (left), and absorption (right) spectra calculated ab initio (solid lines, B3LYP/6-31G*) and within the oscillator model (dashed lines).

be significantly increased if only the benzene chromophore is retained at the same position as that in TPP−Phe. For this case (TPP+C_6H_6, second spectrum from the top in Figure 8), a maximum CD of $\Delta\epsilon_{max} \sim 30$ and the sign in the Soret region already reasonably well approximate the TPP−Phe spectra. Also, the Q band +/− sign pattern around 590 nm was reproduced correctly. The split CD bands of opposite signs induced by the benzene thus reminds one of the effect of the methane; the polarization thus appears as the main mechanism for the CD induction even for the covalently bound chromophore. A similar, albeit weaker, spectral shape can also be induced by the CONHMe residue in the model TPP−CONHMe compound. Here, the electrostatic field of the amide group can contribute to the effect; nevertheless, the benzene alone produced a larger signal. We can conclude that the covalently bound phenylalanine chromophore induces a rather conservative CD spectrum, largely originating in a mutual polarization of the porphyrin and the substituent. A CD signal about 10 times larger in magnitude than that for the unit charge and methane molecule at comparable distances is produced.

Exciton Coupling. Finally, we estimate the effect of the transition coupling in two chirally arranged porphyrin chromophores. A typical pattern can be seen in Figure 9, where absorption (right) and CD (left) spectra of parallel, chirally arranged porphyrins ($\varphi = 45°$) are simulated for four different distances. The ab initio computations are plotted by the solid lines. Several important features can be observed; most striking is the size of the CD ($\Delta\epsilon_{max} \sim 10^3$), which is much larger than that for the previous cases. This suggests that if present, the chiral porphyrin stacking will be the most important mechanism, which is in agreement with general experimental experience.[4,12−14] Also, the effect relatively slowly decays with the porphyrin distance, which corresponds approximately to the dipolar interaction (eq 6). Finally, the CD intensity is roughly conservative, unlike that for the charge perturbation mechanism (cf. Figure 5).

The purely dipolar (TDC) contributions to the spectra are plotted by the dotted lines in Figure 9. The transition energies and dipole moments calculated (B3LYP/6-31G*) for monomer were transferred to the dimer. The spectra were then constructed after the Hamiltonian diagonalization (following eqs 6−8). Clearly, at $d = 10$ Å, the interaction almost totally reduces to the dipole−dipole coupling, as the ab initio (solid line) and TDC (dashed line) spectra are nearly indistinguishable. At $d = 7$ Å, larger deviations start to develop, namely, in the absorption spectrum. At 5 Å, the TDC model provides a notably more split

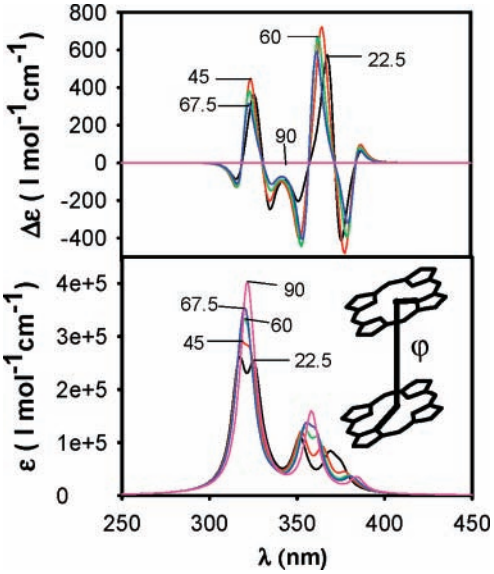

Figure 10. Parallel POR dimer and the dependence of the CD (top) and absorption (bottom) calculated (B3LYP/6-31G*) spectra on the twist angle (φ = ∠NHHN, in degrees, schematically depicted in the figure) for the distance of 5 Å.

absorption Soret profile than TD DFT. This difference further increases for the lowest distance of 4 Å. This is in agreement with the general behavior of the TDC model[42] and can be explained by an increased contribution of the quadrupolar, van der Waals, and other short-range interactions at the shortest distances.

The better agreement of the TD DFT and TDC frequencies in the longest-wavelength region (~360 nm) than that below (e.g., ~270 nm) can be explained by an interaction of the short-wavelength transition with higher excited electronic states implicitly involved in the TD DFT model even though electronic energies are calculated one by one. Indeed, the smaller TD DFT absorption splitting does not lead to smaller CD. On the contrary (left-hand side of Figure 9), the ab initio CD (solid line) is several times larger for d = 4 Å than that obtained from the TDC model.

The angular dependence plotted as computed by the TD DFT model in Figure 10 is not particularly dramatic. The angle of 45° provides the most intense CD signal, although not in the entire wavelength region. Obviously, for negative angles, mirror-image-inversed CD spectra would be obtained, and thus, the angular dependence may be important in the determination of the chirality in experimental studies.[13,14] Perpendicularly oriented and chirally rotated porphyrin dimers provided spectra qualitatively similar to the parallel structures. This can be seen in Figure 11, where CD and absorption is simulated for two distances with the TDC and TD DFT methods. As the perpendicular arrangement prevents a closer contact of the $\pi-\pi^*$ systems, both methods generate virtually the same spectra, and the CD signal is approximately conservative.

Experimental Aspects. Although an interpretation of a specific experiment goes beyond the scope of this work, we can illustrate general features of the induced optical activity on the two types of experimental porphyrin spectra in Figure 12. The Soret CD spectrum of the TPP−Phe molecule[12] (upper panel in the figure) is predominantly positive with two negative side bands. The basic −/+/− pattern is in qualitative agreement with the spectrum of the minimized structure of the same compound as that plotted in Figure 8. The simulated intensity is somewhat larger, but this can be attributed to averaging over

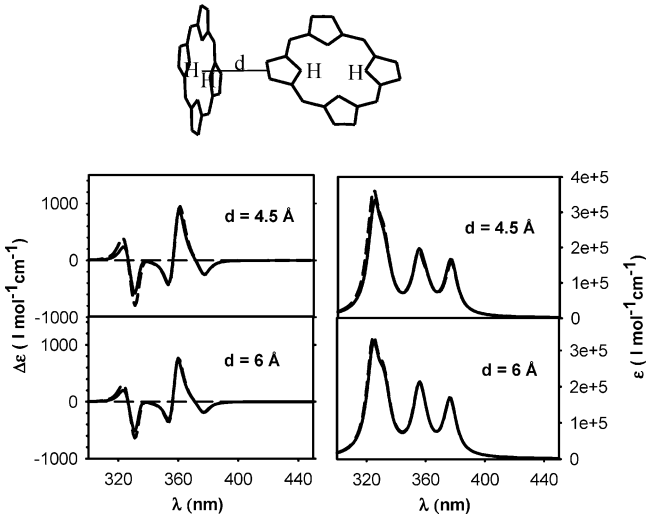

Figure 11. CD (left) and absorption (right) spectra simulated for a perpendicular POR dimer for the two distances indicated in the figure. The left porphyrin was rotated by 45° from a symmetric position. Full lines are used for the ab initio (B3LYP/6-31G*) spectra, and dashed lines are used for the TDC model.

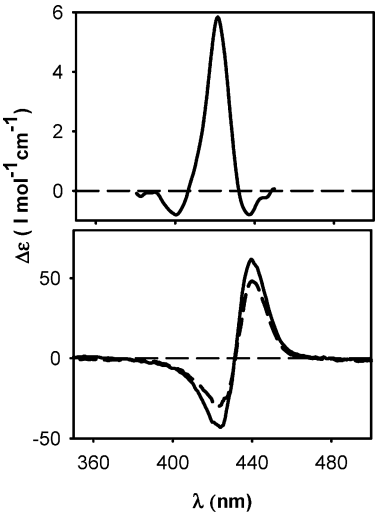

Figure 12. Experimental CD spectra: (top) 5.8 × 10^{-5} M aqueous solution of the TPP-Phe porphyrin[12] and (bottom) the TMPyP (10^{-5} M) complex with the polyglutamic acid (10^{-3} M, pH = 4.8), with and without the presence of copper ions depicted by the full and dashed lines.[43,44]

more conformations and a bigger experimental band width than that used for the simulations.

On the other hand, the TMPyP spectra in the lower panel of Figure 12 represent the case where the CD signal is induced by the TDC mechanism in chirally stacked porphyrin dyes.[6,43,44] The signal is nearly conservative and larger in magnitude by an order bigger than that of the TPP−Phe, as predicted by the computations. The elevating of the porphyrin symmetry to D_{4h} by the copper ions, not explicitly considered in this work, does not seem to have a major effect on the induced CD.

In the future, the ab initio computations can thus improve the reliability of the experimental structural and complexation studies utilizing the induced optical activity in porphyrins and other chromophores. Nevertheless, it should be mentioned that the modeling contains many caveats and is dependent on a general progress of the computational chemistry. The porphyrin stacking, for example, is governed by the van der Waals forces, which is difficult to describe by most of the current DFT functionals.[45,46] In trial computations (not shown), we could

obtain the stable stacked porphyrin dimer only when the Grimme's empirical correction was included.[45] Complex modeling of the macroscopic solvated system, such as the TMPyP spectra in Figure 11, would also be limited by the solvation effects and size of the system. Still, the computations can answer particular questions about local chirality and the underlying mechanisms.

Conclusions

We have investigated the most common mechanisms previously proposed for the optical activity of porphyrins and tested them on model computations utilizing the time-dependent density functional theory. The simplest case of pure electrostatic perturbation providing the smallest CD signal may not be observable in experimental systems. The charge perturbation led to a nonconservative one-sign CD pattern, while the methane molecule induced a conservative CD. Polarization of large functional groups as well as covalently attached residues provide an about 10 times larger CD than that of the electrostatic perturbation. Additionally, this pattern is rather conservative and similar to the transition coupling mechanism. Finally, the transition dipole coupling was determined as the mechanism providing the strongest CD, about 10 times larger than that coming from covalently attached residues. The pure TDC performed well for distant chromophores but exhibited significant deviations from the quantum computations for shorter distances, such as those in parallel stacked porphyrins. These predictions are in agreement with available experimental data. The theoretical modeling can thus significantly contribute to the information about local and global structure obtained in experimental studies where porphyrins are used as chiral probes.

Acknowledgment. The work was supported by the Czech Science Foundation (Grants Nos. 203/06/0420 and 202/07/0732) and the Grant Agency of the Academy of Sciences (A400550702). We thank Ondřej Julínek, Marie Urbanová, and Lucie Bednárová for the experimental spectra.

References and Notes

(1) Pescitelli, G.; Gabriel, S.; Wang, Y.; Fleischhauer, J.; Woody, R. W.; Berova, N. *J. Am. Chem. Soc.* **2003**, *125*, 7613.
(2) Kobayashi, N. *J. Porphyrins Phthalocyanines* **2000**, *4*, 377.
(3) Palivec, L.; Urbanová, M.; Volka, K. *J. Pept. Sci.* **2005**, *11*, 536.
(4) Pančoška, P.; Urbanová, M.; Bednárová, L.; Vacek, K.; Paschenko, V. Z.; Vasiliev, S.; Maloň, P.; Král, M. *Chem. Phys.* **1990**, *147*, 401.
(5) Balaz, M.; DeNapoli, M.; Holmes, A. E.; Mammana, A.; Nakanishi, K.; Berova, N.; Purrello, R. *Angew. Chem., Int. Ed.* **2005**, *44*, 4006.
(6) Hahn, U.; Kaufmann, A.; Nieger, M.; Julínek, O.; Urbanová, M.; Vogtle, F. *Eur. J. Org. Chem.* **2006**, *5*, 1237.
(7) Hamada, D.; Kuroda, Y.; Kataoka, M.; Aimoto, S.; Yoshimura, T.; Goto, Y. *J. Mol. Biol.* **1996**, *256*, 172.
(8) Bracete, A. M.; Kadkhodayan, S.; Sono, M.; Huff, A. M.; Zhuang, C. F.; Cooper, D. K.; Smith, K. M.; Chang, C. K.; Dawson, J. H. *Inorg. Chem.* **1994**, *33*, 5042.
(9) Chiti, F.; Webster, P.; Taddei, N.; Clark, A.; Srefani, M.; Ramponi, G.; Dobson, C. M. *Proc. Natl. Acad. Sci. U.S.A.* **1999**, *96*, 3590.
(10) Burckhardt, G.; Votavová, H.; Jantsch, M.; Zimmer, C.; Lown, J. W.; Schweizer, D. *Cytogenet. Cell Genet.* **1993**, *62*, 19.
(11) Šponar, J.; Votavová, H. *J. Biomol. Struct. Dyn.* **1996**, *13*, 979.
(12) Bednárová, L. Ph.D. Thesis, Charles University, Prague, 1992.
(13) Berova, N.; DiBari, L.; Pescitelli, G. *Chem. Soc. Rev.* **2007**, *36*, 914.
(14) Eguchi, M.; Tachibana, H.; Takagi, S.; Tryk, D. A.; Inoue, H. *Bull. Chem. Soc. Jpn.* **2007**, *80*, 1350.
(15) Bouř, P.; Záruba, K.; Urbanová, M.; Setnička, V.; Matějka, P.; Fiedler, Z.; Král, V.; Volka, K. *Chirality* **2000**, *12*, 191.
(16) Barron, L. D. *Molecular Light Scattering and Optical Activity*; Cambridge University Press: Cambridge, U.K., 2004.
(17) Charney, E. *The Molecular Basis of Optical Activity*; Wiley-Interscience: New York, 1979.
(18) Tinoco, I. *Radiat. Res.* **1963**, *20*, 133.
(19) Snatzke, G. *Angew. Chem., Int. Ed. Engl.* **1979**, *18*.
(20) Snatzke, G.; Kagan, H. *Pure Appl. Chem.* **1979**, *51*, 769.
(21) Jamorski, C.; Casida, M. E.; Salahub, D. R. *J. Chem. Phys.* **1996**, *104*, 5134.
(22) Furche, F.; Ahlrichs, R. *J. Chem. Phys.* **2002**, *116*, 7433.
(23) Stratmann, R. E.; Scuseria, G. E.; Frisch, M. J. *J. Chem. Phys.* **1998**, *109*, 8218.
(24) Autschbach, J.; Ziegler, T.; van Gisbergen, S. J. A.; Baerends, E. J. *J. Chem. Phys.* **2002**, *116*, 6930.
(25) *Circular Dichroism Principles and Applications*; Berova, N., Nakanishi, K., Woody, R. W., Eds.; Wiley-VCH: New York, 2000.
(26) Crawford, T. D.; Tam, M. C.; Abrams, M. L. *J. Phys. Chem. A* **2007**, *111*, 12057.
(27) Dolphin, D. *Porphyrins*; Academic Press: New York, 1979.
(28) Holzwarth, G.; Chabay, I. *J. Chem. Phys.* **1972**, *57*, 1632.
(29) Rogers, D. M.; Besley, N. A.; O'Shea, P.; Hirst, J. D. *J. Phys. Chem. B* **2005**, *109*, 23061.
(30) Rogers, D. M.; Hirst, J. D. *Chirality* **2004**, *16*, 234.
(31) Zhong, W.; Gulotta, M.; Goss, D. J. *Biochemistry* **1990**, *29*, 7485.
(32) Becke, A. *Phys. Rev. A* **1988**, *38*, 3098.
(33) Becke, A. D. *J. Chem. Phys.* **1993**, *98*, 5648.
(34) Šebek, J.; Kejík, Z.; Bouř, P. *J. Phys. Chem. A* **2006**, *110*, 4702.
(35) Ahlrichs, R.; Bar, M.; Baron, H.-P.; Bauernschmitt, R.; Bocker, S.; Deglmann, P.; Ehrig, M.; Eichkorn, K.; Elliott, S.; Furche, F.; Haase, F.; Haser, M.; Horn, H.; Hattig, C.; Huber, C.; Huniar, U.; Kattannek, M.; Kohn, A.; Kolmel, C.; Kollwitz, M.; May, K.; Ochsenfeld, C.; Ohm, H.; Patzelt, H.; Rubner, O.; Schafer, A.; Schneider, U.; Sierka, M.; Treutler, O.; Unterreiner, B.; von Arnim, M.; Weigend, F.; Weis, P.; Weiss, H. *Turbomole*, version 5.8, 5.8 ed.; Quantum Chemistry Group, University of Karlsruhe: Karlsruhe, Germany, 2005.
(36) Frisch, M. J.; Trucks, G. W.; Schlegel, H. B.; Scuseria, G. E.; Robb, M. A.; Cheeseman, J. R.; Montgomery, J., J. A.; Vreven, T.; Kudin, K. N.; Burant, J. C.; Millam, J. M.; Iyengar, S. S.; Tomasi, J.; Barone, V.; Mennucci, B.; Cossi, M.; Scalmani, G.; Rega, N.; Petersson, G. A.; Nakatsuji, H.; Hada, M.; Ehara, M.; Toyota, K.; Fukuda, R.; Hasegawa, J.; Ishida, M.; Nakajima, T.; Honda, Y.; Kitao, O.; Nakai, H.; Klene, M.; Li, X.; Knox, J. E.; Hratchian, H. P.; Cross, J. B.; Bakken, V.; Adamo, C.; Jaramillo, J.; Gomperts, R.; Stratmann, R. E.; Yazyev, O.; Austin, A. J.; Cammi, R.; Pomelli, C.; Ochterski, J. W.; Ayala, P. Y.; Morokuma, K.; Voth, G. A.; Salvador, P.; Dannenberg, J. J.; Zakrzewski, V. G.; Dapprich, S.; Daniels, A. D.; Strain, M. C.; Farkas, O.; Malick, D. K.; Rabuck, A. D.; Raghavachari, K.; Foresman, J. B.; Ortiz, J. V.; Cui, Q.; Baboul, A. G.; Clifford, S.; Cioslowski, J.; Stefanov, B. B.; Liu, G.; Liashenko, A.; Piskorz, P.; Komaromi, I.; Martin, R. L.; Fox, D. J.; Keith, T.; Al-Laham, M. A.; Peng, C. Y.; Nanayakkara, A.; Challacombe, M.; Gill, P. M. W.; Johnson, B.; Chen, W.; Wong, M. W.; Gonzalez, C.; Pople, J. A. *Gaussian 03*, revision C.02; Gaussian, Inc.: Wallingford, CT, 2004.
(37) Eisner, U.; Linstead, R. P. *J. Chem. Soc.* **1955**, 3749.
(38) Wilson, P. J.; Tozer, D. J. *Chem. Phys. Lett.* **2001**, *337*, 341.
(39) Bouř, P. *Int. J. Quantum Chem.* **2003**, *91*, 277.
(40) Šebek, J.; Gyurcsik, B.; Šebestík, J.; Kejík, Z.; Bednárová, L.; Bouř, P. *J. Phys. Chem. A* **2007**, *111*, 2750.
(41) Mennucci, B.; Martínez, J. M. *J. Phys. Chem. B* **2005**, *109*, 9818.
(42) Bouř, P.; Keiderling, T. A. *J. Am. Chem. Soc.* **1992**, *114*, 9100.
(43) Julínek, O.; Goncharova, I.; Urbanová, M. *Supramol. Chem.* **2008**, in press.
(44) Julínek, O. Ph.D. Thesis, Institute of Chemical Technology, Prague, Czech Republic, 2006.
(45) Grimme, S.; Antony, J.; Schwabe, T.; Muck-Lichtenfeld, C. *Org. Biomol. Chem.* **2007**, *5*, 741.
(46) Jurečka, P.; Černý, J.; Hobza, P.; Salahub, D. R. *J. Comput. Chem.* **2007**, *28*, 555.